Journal of
Materials Chemistry B

Accepted Manuscript

ROYAL SOCIETY OF CHEMISTRY

www.rsc.org/materialsB

	People's Hospital Affiliated to Shanghai Jiao Tong University, School of Medicine, Shanghai Key Laboratory of Stomatology, 639 Zhizaoju Road, Shanghai 200011, PR China,

Textual abstract

Copper-incorporated TiO_2 coating on titanium surface can significantly enhance the antimicrobial, angiogenic and osteogenic activities.

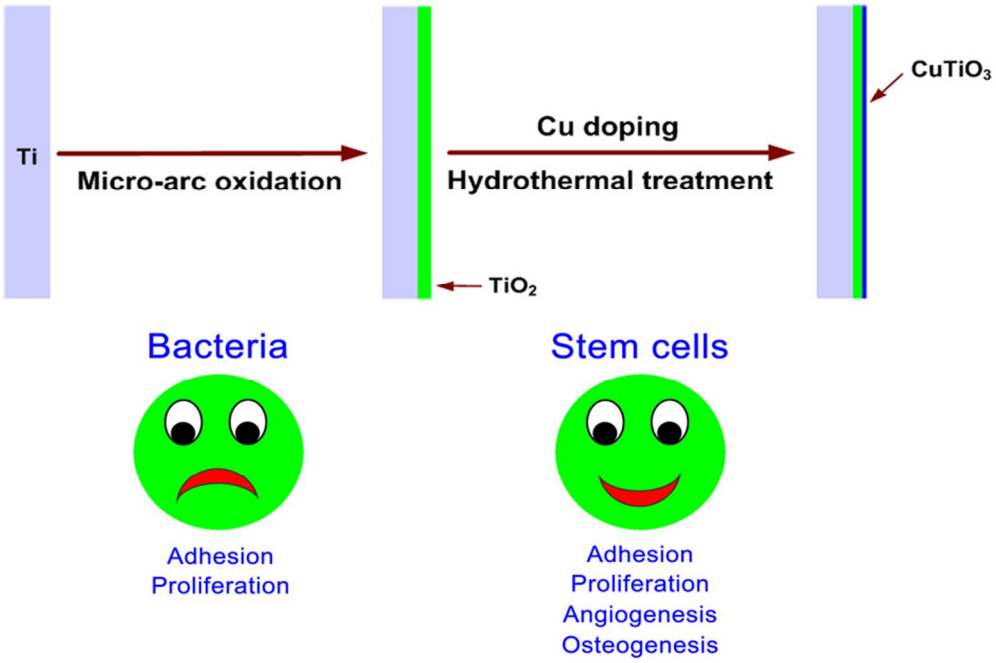

Copper-incorporated TiO2 coating on titanium surface can significantly enhance the antimicrobial, angiogenic and osteogenic activities.
40x26mm (600 x 600 DPI)

Antibacterial property, angiogenic and osteogenic activity of Cu-incorporated TiO_2 coating

Qianju Wu[a, b,1], Jinhua Li[c,1], Wenjie Zhang[a,b], Haixin Qian[a], Wenjun She[a], Hongya Pan[b], Jin Wen[a,b], Xiuli Zhang[b], Xuanyong Liu[c,*] and Xinquan Jiang[a,b,*]

[a] Department of Prosthodontics, Ninth People's Hospital affiliated to Shanghai Jiao Tong University, School of Medicine, 639 Zhizaoju Road, Shanghai 200011, China.

[b] Oral Bioengineering Lab, Ninth People's Hospital Affiliated to Shanghai Jiao Tong University, School of Medicine, Shanghai Key Laboratory of Stomatology, 639 Zhizaoju Road, Shanghai 200011, China.

[c] State Key Laboratory of High Performance Ceramics and Superfine Microstructure, Shanghai Institute of Ceramics, Chinese Academy of Sciences, Shanghai 200050, China.

Corresponding Authors:

Prof. Xinquan Jiang

Department of Prosthodontics, Ninth People's Hospital affiliated to Shanghai Jiao Tong University, School of Medicine, 639 Zhizaoju Road, Shanghai 200011, China.

E-mail: xinquanj@aliyun.com

Tel.: +86 21 63135412. Fax: +86 21 63136856.

Prof. Xuanyong Liu

State Key Laboratory of High Performance Ceramics and Superfine Microstructure, Shanghai Institute of Ceramics, Chinese Academy of Sciences, Shanghai 200050, China.

E-mail: xyliu@mail.sic.ac.cn

Tel.: +86 21 52412409. Fax: +86 21 52412409.

[1] These authors contributed equally to this work.

Abstract

Numerous efforts have been made to modify the surface topography and chemical composition of biomedical implants in order to enhance the antibacterial ability and the osteointegration between implants and surrounding bone tissue. In the present work, copper-incorporated TiO_2 coatings were fabricated by combining micro-arc oxidation and hydrothermal treatment together to functionalize the surface of Ti implants. The as-prepared surfaces exhibited a hierarchical structure comprising nanoneedles nearly perpendicular to the microrough surface of TiO_2 coating. The Cu-loaded TiO_2 coating possessed strong antimicrobial ability against Gram-negative Escherichia coli. In vitro cytocompatibility evaluation suggests that no significant cytotoxicity appeared on Cu-incorporated TiO_2 coating. Furthermore, the addition of copper element could stimulate the expression of angiogenic genes including hypoxia-inducible factor-1α (HIF-1α) and vascular endothelial growth factor (VEGF) in rat bone marrow stem cells (BMSCs). Meanwhile, they tended to undergo osteogenic differentiation, indicated by the up-regulation expression of osteogenic markers and the higher level of alkaline phosphatase activity. This study provides insight for the surface modification of biomedical Ti-based implants. To our best knowledge, this is a successful attempt for the first time to combine micro-arc oxidation and hydrothermal treatment to introduce copper nutrient element to functionalize Ti-based implant surfaces with enhanced angiogenesis potential, osteostimulation and antimicrobial property that can better meet the clinical needs.

Keywords: titania; copper; antibacterial; angiogenesis; osteogenesis; stem cells

1. Introduction

Oral implantation is the most innovative and superior treatment for both partially and completely edentulous patients due to the stability and superiority compared with the removable dentures, which often cause leveraging, allergic reaction to the materials used and alveolar bone resorption for a long term. Commercially titanium and its alloys have been extensively used for dental and orthopedic implants because of their intrinsic biocompatibility and excellent mechanical strength.[1] However, Ti-based materials cannot achieve sufficient osseointegration due to the suboptimal osteoconductivity.[2] Moreover, the surface of Ti-based implants may provide substrates for bacteria to adhere, colonize, and subsequently form biofilms, leading to the infections at the implant sites, which is another main reason for surgery failure.[3]

In order to solve the above problems, increasing researches have focused on the surface loading of antibacterial agents to prevent bacterial adhesion at the implant sites and the surface modification to enhance ossteointegration between implant surface and surrounding bone tissue.[4] As is known, copper (Cu) has excellent antibacterial properties against numerous bacteria,[4-6] and it delivered by far the best compromise between antibacterial effectiveness and cytotoxicity when compared with other antibacterial ions such as Zn, Ag.[7] Incorporation of copper into medical devices to enhance their antibacterial activity has drawn considerable attentions. Ren et al. had developed the Cu-bearing stainless steel, which not only maintained the excellent mechanical and corrosion-resistant properties, but also showed strong antibacterial ability by inhibiting the formation of bacterial biofilms on surface.[8] Additionally, it

has been demonstrated that there is an intimate relationship between copper levels and vascularization by stimulating the proliferation of endothelial cells and promoting the up-regulation of VEGF,[9, 10] which is a key factor for vascularization. Moreover, copper takes part in bone metabolism and is beneficial to the bone formation.[11] Studies have reported that trace amount of copper (50 μM) can promote the osteogenic ability of MSC obtained from postmenopausal women.[12] Ewald et al. found that Cu-CPC could enhance the cell activity and proliferation of osteoblastic cells.[13] It can offer a promising alternative to incorporate copper ions into biomaterials in order to stimulate cellular activity for improving bone healing.

However, extra attention should be paid to the cytotoxic effects of the copper ions released from biomedical devices.[14] Hence, it is essential to establish a unique sustained release platform that can keep copper ions in a state of trace amount to reduce the adverse effects against the surrounding tissue in order to promote implant ingrowth and maintain the antibacterial properties.

Applying the approach of micro-arc oxidation (MAO) to modify the implant surface to enhance its biocompatibility and osteoconductivity has been widely investigated. MAO, based on the principle of plasma-electrolytic oxidation, forms a rough, firmly adherent TiO_2 layer on Ti surface.[15, 16] And meanwhile, bioactive elements such as calcium (Ca), phosphorus (P), which are compositions of bone, can electrolytically deposit into the surface layer, and the incorporation of Ca or P elements into TiO_2 film can enhance the activity of osteoblastic cells and promote the more rapid formation of new bone in vivo.[17] Moreover, Studies have demonstrated the

inorganic ions incorporated into porous TiO_2 coating fabricated by MAO could show a sustained release pattern, instead of burst release.[18, 19] Taking these into consideration, it is expected that the superiority and biocompatibility of calcium/phosphate-rich TiO_2 coating could "compensate" the cytotoxcity of copper ions, making a balance between antibacterial property and biocompatibility.

In the present work, hierarchical calcium/phosphate-rich TiO_2 coating with micro/nano topography was fabricated on metallic Ti surface via MAO method and subsequently copper ions were doped into the MAO-treated surface by hydrothermal treatment. The antibacterial activity of the coatings against Gram-negative Escherichia coli (E. coli) was examined. Furthermore, BMSCs were seeded onto the modified surfaces to investigate whether the combination of TiO_2 coating with copper ions could possess favorable cytocompatibility, angiogenesis and osteogenesis potentials. This study may provide a new sight for the better understanding and designing of copper incorporated-based surface modification for biomedical Ti-based implants to improve their biological performances and success rates.

2. Materials and methods

2.1. Samples preparation and modification

Commercially pure Ti (Cp Ti, Grade 1, > 99.85 wt% purity) foils with dimensions of 10 mm × 10 mm × 1 mm or 20 mm × 20 mm × 1 mm were ultrasonically cleaned several times, then pickled in 5 wt% oxalic acid solution at 100

℃ for 2 h to eliminate the oxide layer and acquire a clean and homogeneous surface, followed by ultrasonically cleaning and drying for further use.[20] TiO_2 coatings were prepared on Ti surface by micro-arc oxidation in calcium/phosphate-containing electrolyte with calcium acetate monohydrate ($C_4H_6O_4Ca \cdot H_2O$), glycerophosphate disodium salt pentahydrate ($C_3H_7Na_2O_6P \cdot 5H_2O$). Copper ions were hydrothermally doped into the TiO_2 coatings. Briefly, each MAO-treated Ti foil was immersed in 10 nM or 100 nM $CuCl_2$ aqueous solution in a Teflon-lined reaction vessel at 200 ℃ for 1 hour. After the reaction vessel naturally cooled to room temperature, the Ti foils were gently rinsed with deionized water and then dried in ambient atmosphere. The whole preparation process for Cu-incorporated TiO_2 coating is illustrated in **Scheme 1**. And the resulting samples were denoted as TiO_2, 10nM-Cu and 100nM-Cu, respectively.

2.2. Surface characterization

The surface morphology was characterized by field-emission scanning electron microscopy (FESEM; S-4800, HITACHI, Japan). The crystallinity of the coatings was studied using an X-ray diffractometer (XRD; D/Max, Rigaku, Tokyo, Japan) fitted with a Cu Kα (λ = 1.541 Å) source at 40 kV and 100 mA, in the range of 2θ = 15 °~ 80 °with a step size of 0.02 °. Phase identification was carried out with the help of the standard JCPDS database. In the X-ray diffraction experiment, the glancing angle of the incident beam against the surface of the specimen was fixed at 1 °. The chemical compositions and chemical states of the titanium surfaces were determined

by X-ray photoelectron spectroscopy (XPS; PHI 5802, Physical Electronics Inc, Eden Prairie, MN) with an Mg Kα (1253.6 eV) source.

2.3. Ions release determination

The TiO_2, 10nM-Cu, and 100nM-Cu specimens were immersed in 10 mL Dulbecco's Modified Eagle's medium (DMEM, Gibco, USA) at 37 ℃ for 1, 4, 7 and 14 days successively. At the end of incubation, the leaching liquid was collected and the concentrations of Ca/P/Cu/Ti(IV) ions being released were measured by inductively-coupled plasma mass spectrometry (ICP-MS; Nu Instruments, Wrexham, UK).

2.4. Antibacterial activity evaluation

The antimicrobial effect of TiO_2, 10nM-Cu, and 100nM-Cu specimens was evaluated by bacterial counting method using Escherichia coli (E. coli, ATCC 25922). The specimens were sterilized in 75 v/v% ethanol aqueous solution for 2 hours. A solution containing the bacteria at concentration of 10^7 CFU/mL was introduced onto the specimen to a density of 60 μL/cm^2. The specimens with bacterial solution were incubated at 37 ℃ for 24 h. The dissociated bacterial solution was collected and inoculated into a standard agar culture medium. After incubation at 37 ℃ for another 24 h, the live bacteria were counted in accordance with the National Standard of China GB/T 4789.2 protocol and the antibacterial ratio was calculated using the formula, $A.R. = (A - B) / A \times 100\%$, where *A.R.* means the antibacterial ratio; *A* is the

average number of bacteria on the control specimen (CFU/specimen); *B* is the average number of bacteria on the testing specimen (CFU/specimen).

In the SEM examination, a bacterial solution at the concentration of 10^7 CFU/mL was put on the specimen to a density of 60 μL/cm^2, incubated at 37 ℃ for 24 h, fixed, and dehydrated in a series of ethanol solutions (30, 50, 75, 90, 95, and 100 v/v%) for 10 min each sequentially, with the final dehydration conducted in absolute ethanol (twice) followed by drying in the hexamethyldisilizane (HMDS) ethanol solution series.

2.5. Culture of rat bone marrow stem cells (BMSCs)

Bone marrow stem cells were isolated and cultured from 8-week-year-old male Wistar rats according to our previously established procedures.[21] All experimental protocols of animals in this study were approved by the Animal Care and Experiment Committee of the 9th People's Hospital, which is affiliated to Shanghai Jiao Tong University School of Medicine. Briefly, after cutting off both ends of rat femurs at the epiphysis ,the bone marrow was rinsed out using Dulbecco's modified Eagle's medium (DMEM, Gibco, USA) supplemented with 10% fetal bovine serum (Gibco, USA) and 200 U/mL heparin (Sigma, USA). Primary Cells were cultured in Dulbecco's modified Eagle's medium supplemented with 10% fetal bovine serum, 100 U/mL streptomycin, and 100 U/mL of penicillin, with an atmosphere of 5% CO_2 at 37 ℃. The culture medium was changed after 24 hours to remove nonadherent cells and then renewed three times each week. Cells at passage 2~3 were used for further

studies.

2.6. Cell proliferation activity assay

The cell proliferation activity assay of the BMSCs on different samples was evaluated by 3-(4,5-dimethylthiazol-2-yl)-2,5-diphenyl tetrazolium bromide (MTT) colorimetric assay. Initially, 2.0×10^4 cells per mL were seeded onto each flat sample in a 24-well plate for 1, 4 and 8 days of culture. At each time point, 40 μL MTT solution (5 mg/mL) was added and incubated for 4 hours at 37 ℃ to form formazan. Finally, the formazan was dissolved in dimethyl sulfoxide (DMSO) and the absorbance was measured at 490 nm using an ELX ultra microplate reader (BioTek, Winooski, VT). All experiments were performed in triplicate.

2.7. Cell morphology

The cell morphology of BMSCs after 48 hours of culture on specimens were observed by scanning electron microscopy (SEM) and immunofluorescence technique. The specimens were washed three times with phosphate buffered saline (PBS), fixed in 3% glutaraldehyde for 12 h at 4 ℃. Then they were washed three times with PBS to remove glutaraldehyde and then dehydrated in the increased grade concentrations of ethanol (from 30, 50, 75, 90, 95, to 100 v/v%), followed by air-drying in hexamethyldisilizane before being sputter-coated with platinum and finally observed through a scanning electron microscope (SEM, S-3400, HITACHI, Japan).

As for immunofluorescence assay，the BMSCs cultured on samples were fixed in

4% paraformaldehyde for 30 min and washed with PBS, subsequently treated with 0.1%Triton X-100 to permeabilize the cell membranes and then blocked with 1% BSA for 30 min. The actin cytoskeletons were labeled by staining with FITC-Phalloidin (Sigma, USA), while the cell nuclei were counterstained with 4',6-diamidino-2-phenylindole dihydrochloride（DAPI，Sigma, USA). All specimens were visualized using immunofluorescence microscopy (Olympus, BX51, Japan).

2.8. Alkaline phosphatase (ALP) activity assay

After being cultured for 14 days in DMEM, the BMSCs on different substrates were fixed with 4 % paraformaldehyde and stained using an alkaline phosphatase kit according to the manufacturer's instructions (Shanghai Hongqiao Medical Reagent Company, Shanghai, China). For alkaline phosphatase (ALP) quantitative assay, cells seeded on different samples were incubated with p-nitrophenyl phosphate (pNPP) (Sigma, St. Louis, MO, USA) at 37 ℃ for 30 min and ALP activity was detected by the measurement of optical density (OD) values at 405 nm, while total protein content was measured with the Bradford method at 630 nm of optical density (OD) values according to a series of bovine serum albumin (BSA, Sigma, USA) standards. Finally, ALP activity levels were normalized to the total protein content and expressed as OD values at 405 nm per milligram of total cellular proteins. All the measurements were made in triplicate.

2.9. Quantitative real-time PCR assay

At the time point of 14 days, cells seeded on each flat sample were collected and resuspended in Trizol reagent (Invitrogen, USA), and the total RNA was harvested to synthesize complementary DNA using a PrimeScript 1st Strand cDNA Synthesis kit (Takara, Japan) according to the manufacturer's instructions. The expression of key angiogenic factors (HIF-1α and VEGF) and osteogenic differentiation markers osteopontin (OPN), bone morphogenetic protein-2 (BMP-2) and collagen type 1 (Col-1) in three groups were measured by using reverse transcription polymerase chain reaction (RT-PCR) with Bio-Rad MyiQ single color Real-time PCR system, while the housekeeping gene, β-actin, was used for normalization. Purified gene-specific primers above were synthesized commercially (Shengong, Co. Ltd., Shanghai, China) and the primer sequences used in present study are listed in **Table 1**. All experiments were performed in triplicate to obtain the average data.

2.10. Statistical analysis

Statistical comparisons were measured via one-way ANOVA and SNK post hoc based on the normal distribution and equal variance assumption test. All statistical analysis was carried out using an SAS 8.2 statistical software package (Cary, USA). All the data are expressed as means ± standard deviation (SD). Values of *$p < 0.05$, **$p < 0.01$ or ##$p < 0.01$ were considered statistically significant. Notes: *$p < 0.05$, **$p < 0.01$ versus control TiO_2 group, ##$p < 0.01$ versus 10nM-Cu group.

3. Results

3.1. Characterization of specimens

Figure 1 shows the surface topographies of Ti plates after undergoing micro-arc oxidation and subsequent hydrothermal treatment. A rough porous structure was formed on Ti surface by micro-arc oxidation, as shown in **Figure 1A**. These pores were well separated with each other and homogeneously distributed over the coating surface. However, the Ti surface exhibited a relatively smooth morphology under high magnification (**Figure 1B**). Combining with the XRD pattern in **Figure 2**, the as-prepared coating on Ti surface mainly consists of anatase TiO_2, as well as tiny peaks related to rutile TiO_2. In detail, as attributive indicators of TiO_2 anatase phase, typical diffraction peaks were at $2\theta = 25.2°$, $38.0°$, $48.1°$, $53.8°$, $62.8°$, etc., and for the rutile phase a small peak at $2\theta = 27.4°$.[22] After reacting with 10 nM $CuCl_2$ under hydrothermal conditions, the surface topography at low magnification was almost not altered at all (**Figure 1C**); while at high magnification, unique homogeneous nanoneedle morphology appeared, nearly perpendicular to the surface, as shown in **Figure 1D**. With regard to the hydrothermal reaction with 100 nM $CuCl_2$, the low-magnification topography produced by micro-arc oxidation still maintained well (**Figure 1E**), accompanied by the emergence of nanoneedle structure at high magnification as well (**Figure 1F**). If $CuTiO_3$ phase exist, its main peak will overlap with that of anatase.[23]

The XPS full spectra obtained from the surfaces of TiO_2, 10nM-Cu and 100nM-Cu are shown in **Figure 3A**. On the basis of the XPS results, titanium (Ti),

oxygen (O), calcium (Ca) and phosphorus (P) elements were detected on the Ti surface after micro-arc oxidation. After the hydrothermal treatment in $CuCl_2$ aqueous solution (10 nM and 100 nM), the copper (Cu) element was also determined on the treated specimens, with content of 0.4 wt % and 0.9 wt %, respectively. From this figure, it also can be seen that during the hydrothermal treatment, both Ca and P elements were suffered from some loss. High-resolution XPS analysis was further performed for the 100nM-Cu specimen. The Ti 2p XPS spectrum in **Figure 3B** shows two peaks centered at around 464.2 eV and 458.6 eV corresponding to Ti $2p_{1/2}$ and Ti $2p_{3/2}$ in titanate or TiO_2, respectively.[20] The O 1s XPS spectrum was divided into two Gaussian component peaks (**Figure 3C**), among which the peak located at 530.1 eV is assigned to the O atoms bound to metal atoms such as Ti, Cu, etc.,[24] and the other peak at 531.3 eV corresponds to the O 1s in P=O— groups from $Ca_3(PO_4)_2$ or $CaHPO_4$.[25, 26] The P 2p peaks located at 133.5 eV and 132.4 eV were in consistent with the P–O bonds in PO_4^{3-} and HPO_4^{2-}, respectively.[26, 27] In regard to the Ca 2p XPS spectrum, three peaks were fitted with the predominant ones at 347.1 eV and 350.7 eV corresponding to Ca 2p in $Ca_3(PO_4)_2$,[28, 29] and the third one at 347.5 eV assigned to $CaHPO_4$.[30] As for the Cu 2p spectrum, the double peaks at 932.7 eV and 952.7 eV were assigned to the Cu $2p_{3/2}$ and Cu $2p_{1/2}$ in $CuTiO_3$ ($CuO \cdot TiO_2$), respectively.[31, 32]

The release characteristics of Ca, P and Cu ions from their corresponding specimens soaked in DMEM are shown in **Figure 3G-I**. During the 14 days, Ca/P/Cu ions were released from each specimen sustainedly. From this figure, the release rate

and total release amount of Cu^{2+} ions from the 100nM-Cu surface was significantly higher than those from the 10nM-Cu surface. The release features of these ions were in accordance with the surface XPS analysis. At the same time, the dissolution of Ti(IV) ions from the specimens was not detected, implying that Ti(IV), Ca, P and Cu ions did not dissolve congruently.

3.2. Antimicrobial performance

The dissociated E. coli bacteria were recultivated on agar according to bacterial counting method. **Figure 4A-B** shows the typical photographs for the count of bacterial colonies on the control and test groups and the corresponding bacterial counting results. It can be seen that, E. coli can grow well on the surface of the pristine micro-arc oxidized TiO_2 coating, indicating the non-existent antibacterial ability. After the copper doping by hydrothermal reaction, the Cu-incorporated TiO_2 coatings (10nM-Cu and 100nM-Cu) have a strong capability to destroy the viability of E. coli, especially for the 100nM-Cu group, further enhancing the antimicrobial property. SEM observation was further utilized to identify the morphology and membrane integrity of the E. coli bacteria. Most of the bacteria on TiO_2 coating surface possessed intact cytoplasmic membranes and intercellular communication junctions (red arrow in **Figure 4D**), indicating the exuberant vitality of E. coli.[33] With regard to the Cu-incorporated TiO_2 coatings, i.e., 10nM-Cu and 100nM-Cu groups, prevalent cell lysis and cytoplasma leakage existed on the surfaces, more severe for 100nM-Cu (red arrows in **Figure 4F**, **H**), indicating that E. coli can hardly survive on

the Cu-incorporated TiO_2 coatings. These observations were quite consistent with the bacterial counting results. The results show that the death of E. coli on the Cu-incorporated TiO_2 coatings can be attributed to the disruption of membrane integrity, exerting the potent antibacterial performance by copper incorporating.

3.3. Cell proliferation and morphology

The MTT results in **Figure 5** shows the proliferation and viability of BMSCs on various samples. From this figure, it is obvious that, there was an increasing trend of cell growth throughout the whole culture period. No statistically significant difference was found among the three groups at each time point which demonstrated that the Cu-incorporated TiO_2 coatings have no significant cytotoxicity, suitable for the subsequent in vitro study.

In order to observe cell adhesion and spreading, BMSCs cultured on different samples were examined by SEM and immunofluorescence microscopy after 2 days of culture. The SEM results show that Cu-incorporated TiO_2 coatings can support BMSCs attachment and cells appeared to spread out extensively, even covering the micropores on the surfaces, as indicated by the red arrows in **Figure 6B-C**. Cytoskeletons were labeled to observe the cell morphology of seeded BMSCs by immunofluorescence microscopy, as shown in **Figure 7**. The cells attached on each samples exhibited similar fibroblastic morphology with the well-organized cytoskeleton structure. From the observations, it can be inferred that the incorporation of copper ions into TiO_2 coating did not hinder the initial adhesion and spreading of BMSCs in comparison

with the control group.

3.4. Alkaline phosphatase (ALP) activity

ALP staining was performed for BMSCs after culturing on the three groups for 14 days. From this figure, the most intense ALP staining was found for cells cultured on 100nM-Cu group (**Figure 7C**), followed by 10nM-Cu group (**Figure 7B**), when compared with that on the pristine TiO_2 coating (**Figure 7A**). Moreover, the quantitative analysis results revealed that the ALP activity for the cells cultured on 10nM-Cu and 100nM-Cu groups was significantly higher than that on the control TiO_2 group with statistically significant difference $^*p < 0.05$ and $^{**}p < 0.01$, respectively, and 100nM-Cu group showing the highest level of ALP activity with statistically significant difference $^{\#\#}p < 0.01$ compared with 10nM-Cu group.

3.5. Angiogenesis and osteogenesis activity

Quantitative real-time PCR assay was performed to detect the key angiogenic factors and osteogenic-related markers for BMSCs after culturing on various samples for 14 days (**Figure 8**). The β-actin was used for normalization and the results were expressed as relative expression levels to the control TiO_2 group.

Figure 8A-B shows that the incorporation of copper ions into micro-arc oxidized TiO_2 coatings (10nM-Cu and 100nM-Cu groups) can remarkably increase the expressions of HIF-1α and VEGF than the pristine coating, indicating the promotion function of copper element on angiogenesis activity in certain content range. At the

same time, the copper doping also can significantly enhance the osteogenic differentiation of BMSCs, indicated by the up-regulated expressions of bone-related genes (OPN, BMP-2 and Col-1). The BMSCs cultured on 100nM-Cu group had the most significant enhancement for the markers of angiogenesis and osteogenesis compared to the other two groups.

4. Discussion

Nowadays, a sole surface modification method cannot meet all the clinical requirements, such as inhibiting bacterial infections, enhancing osseointegration, promoting angiogenesis, etc.,[34, 35]. To achieve the multifunctional purposes and meet the clinical applications, it is a tendency to combine various modification methods together to functionalize the surface of metallic biomaterials. Micro-arc oxidation (MAO) is a facile, controllable, and cost-effective surface modification method and large amounts of investigations on the biological performances of TiO_2 coatings on implants derived from MAO have suggested its promising applications in orthopedic and dental clinical work.[36, 37] Copper ions have been demonstrated to possess excellent antibacterial property and closely link with vascularization. More interestingly, it was recently reported that copper ions could promote the collagen deposition during the osteogenesis process.[38] Due to the simplicity and flexibility of regulating surface morphology and chemical element, hydrothermal modification is considered as a promising chemical method for functionalizing Ti-based biomaterials.[20] In the present work, in order to optimize the experimental design and

explore the appropriate concentrations of copper ions to provide guidance for the subsequent incorporation into TiO_2 coating by hydrothermal method, a primary research on the role of copper ions with different concentrations for the biological activities of BMSCs derived from rats was performed (See supplementary information), and then the novel Cu-incorporated TiO_2 coatings with tunable Cu loadings were prepared by micro-arc oxidation and hydrothermal treatment to combine the biological functions of copper nutrient element and titanium oxide layer to exert the synergistic effect. Recently, Huo et al.[39] developed a facile strategy to modify titanium surface by anodization to fabricate TiO_2 nanotubes, followed by hydrothermal treatment in zinc salt solution to produce $ZnTiO_3$, thus significantly enhancing the osteogenic activity and antibacterial ability. During the hydrothermal process, the hydrolysis process of copper ions (Cu^{2+}) with water molecule (H_2O) proceeds as follow,

$$Cu^{2+} + 2H_2O \rightarrow Cu(OH)_2 + 2H^+ \quad (1)$$

This reaction can be accelerated at high temperature and high pressure under the hydrothermal condition, resulting in the acidic environment. As TiO_2 is an amphoteric oxide, the surface is enriched with Ti-OH groups and the main species on the surface of MAO coating is OH_2^+, thus producing a positively charged surface.[40] Contributed by electrostatic adsorption, the $Cu(OH)_2$ hydrolysate got enriched on the OH_2^+-terminated surface and reacted with TiO_2 to form $CuTiO_3$ as follow (**Scheme 1**),

$$Cu(OH)_2 + TiO_2 \rightarrow CuTiO_3 + H_2O \quad (2)$$

The obtained experimental results show that micro-arc oxidized TiO_2 coatings had numerous micropores. After being hydrothermally treated by $CuCl_2$ solutions at concentrations of 10 nM and 100 nM, the coating surfaces exhibited a hierarchical structure, with abundant nanoneedles nearly perpendicular to the microrough surfaces of TiO_2 coatings. Since the excessive doses of copper ions may cause certain cytotoxicity, it must be prudent to control over the release rate of copper ions from implants surface.[41] In this work, the release feature of copper ions from the Cu-incorporated TiO_2 coatings was measured by ICP-MS, showing that both 10nM-Cu and 100nM-Cu can maintain a sustained release of copper ions with the concentrations much lower than those causing cytotoxic effect reported in previous literatures.[42-45] It indicates that micro-arc oxidized porous TiO_2 coatings can serve as a promising loading platform enabling the controlled release of copper ions to minimize cytotoxicity and maintain other biological functions like antimicrobial property. In fact, the Cu-incorporated TiO_2 coatings were demonstrated here to possess good antibacterial activity, suggesting its great potential for the prevention of implant-associated infections. Nowadays, with the rising concerns on antibiotic-resistant pathogens, especially some bacterial strains like superbug NDM-1 having developed the resistance against known antibiotics,[46] self-antibacterial materials targeting membrane functions have huge potential to diminish bacterial infections.[47] Copper ions can damage respiratory enzymes and extract electrons from bacterial membranes, thus causing cell lysis, cytoplasm leakage and bacteria death.[48]

It is widely accepted that the interactions between cells and biomaterials plays an

important role in tissue engineering and the biologic behaviors of cells are mainly influenced by surface topography and chemistry.[40, 49, 50] This study was attempted to investigate the interactions between surface cues and BMSCs, an ideal one for the tissue engineering of bone regeneration. It turns out to be that the Cu-incorporated TiO_2 coatings are favorable for the cells adhesion, extraordinarily stretching with the well-organized cytoskeleton structure on the coating surfaces. Meanwhile, cell proliferation shows an upward trend with the time dependent manner for each group, indicating the prepared Cu-incorporated TiO_2 coatings possess good cytocompatibility without significant cytotoxic effect on BMSCs viability.

Numerous studies have revealed that copper can significantly stimulate new vessel formation, and a widely accepted mechanism is that copper can stabilize hypoxic microenvironment and subsequently involve in the activation of VEGF which is associated with neovascularization and tissue regeneration.[9, 51-53] However, it is still unclear whether copper incorporating into TiO_2 coatings is capable of inducing the angiogenesis function. In the present work, 10nM-Cu and 100nM-Cu can remarkably promote the up-regulation expressions of HIF-1α and VEGF of BMSCs, which suggests the stimulatory effect of copper on vascularization as we expected and lay a solid foundation for preparing angiogenesis-enhanced bioactive implant coatings. More interestingly, the obtained results show that the expressions of bone-related genes, including osteogenic markers OPN, BMP-2 and Col-1, were significantly promoted when culturing BMSCs on the Cu-incorporated TiO_2 coatings. Meanwhile, ALP activity of BMSCs on the coatings increased with copper loading ascending,

indicating the potential beneficial effect of copper element on the differentiation and mineralization of BMSCs. Previous studies have suggested that osteogenesis and angiogenesis are closely coupled and their interaction is controlled by a precise network of different growth factors, such as HIF-1α and VEGF.[54] Hence, we speculate that the angiogenesis effect of copper nutrient element plays a central role to stimulate the ALP activity and the osteogenic gene expression of BMSCs. Nevertheless, the mechanism of facilitating osteogenic gene expression is still unclear and needs to be elucidated further.

The current technologies to modify implants surfaces emphasize not only in chemistry composition but also from the aspect of topography, and modification of one single element may not be sufficient to achieve satisfactory results. As is known to all, cell-biomaterial interaction plays a crucial role in the promotion of early stages of cellular responses and the effects of hierarchical micro/nanoscale structures on cell adhesion have been reported by several studies[49,50]. On the other hand, Cu ions, performing as biofunctional elements, could improve the biological performances of cell after releasing from the substrates to alter the local micro-environment, which had been confirmed in the present study. Therefore, we believe the combination of these two factors contributes simultaneously and synergistically to the superior biofunctionality of biomedical implants coating in vitro.

From the obtained results of our work, it seems to be a feasible way to incorporate copper element into micro-arc oxidized TiO_2 coatings by hydrothermal treatment and the Cu-incorporated TiO_2 coatings can act as a stable system to maintain the sustained

release pattern of copper ions. To our knowledge, it still remains a significant challenge to develop bioactive multifunctional coatings on implants surfaces to improve the success rates of implant surgery. The prepared Cu-incorporated TiO_2 coatings in this work not only offer implants good antibacterial property, but also improve the angiogenesis potential and further enhance the osteogenic differentiation ability of BMSCs, suggesting the potential for promoting implant osteointegration. Of course, further in vivo investigations are needed for clinical applications.

5. Conclusions

In this study, we successfully prepared a novel bioactive coating on metallic titanium surface, i.e., Cu-incorporated TiO_2 coating, by combining micro-arc oxidation and hydrothermal treatment, which can act as a delivery platform for the sustained release of copper ions. Furthermore, the obtained Cu-incorporated TiO_2 coating on titanium was demonstrated to possess multifunctional characteristics of enhanced antimicrobial, angiogenesis and osteostimulation capabilities. To the best of our knowledge, this is a successful attempt for the first time to apply the combination of micro-arc oxidation and hydrothermal treatment to introduce the trace element copper for the surface functionalization of biomedical Ti-based materials, which can be of great potential for the dental and orthopedic applications.

Acknowledgements

Joint financial support from the National Basic Research Program of China (973

Program, 2012CB933600), National Science Fund for Distinguished Young Scholars (81225006), Chang Jiang Scholars Program, National Natural Science Foundation of China (81271704, 31370962), and Shanghai Science and Technology R&D Fund (11JC1413700, 13441902400) is acknowledged.

Notes and references

Electronic Supplementary Information (ESI) available: [details of any supplementary information available should be included here]. Additional data from exploratory experiments on BMSCs proliferation and viability, osteogenesis and angiogenesis activities, and surface morphology of samples (**Figures S1-S4**) to optimize the concentrations of $CuCl_2$ solution used in hydrothermal reaction. See DOI:

1 W. Zhang, Z. Li, Y. Liu, D. Ye, J. Li, L. Xu, B. Wei, X. Zhang, X. Liu and X. Jiang, *International journal of nanomedicine*, 2012, **7**, 4459-4472.

2 W. Zhang, G. Wang, Y. Liu, X. Zhao, D. Zou, C. Zhu, Y. Jin, Q. Huang, J. Sun, X. Liu, X. Jiang and H. Zreiqat, *Biomaterials*, 2013, **34**, 3184-3195.

3 J. Li, X. Liu, Y. Qiao, H. Zhu and C. Ding, *Colloids and surfaces. B, Biointerfaces*, 2013, **113C**, 134-145.

4 S. Kalaivani, R. K. Singh, V. Ganesan and S. Kannan, *Journal of Materials Chemistry B*, 2014, **2**, 846-858.

5 N. Matsumoto, K. Sato, K. Yoshida, K. Hashimoto and Y. Toda, *Acta biomaterialia*, 2009, **5**, 3157-3164.

6 E. A. Neel, I. Ahmed, J. Pratten, S. N. Nazhat and J. C. Knowles, *Biomaterials*,

2005, **26**, 2247-2254.

7 F. Heidenau, W. Mittelmeier, R. Detsch, M. Haenle, F. Stenzel, G. Ziegler and H. Gollwitzer, *Journal of materials science. Materials in medicine*, 2005, **16**, 883-888.

8 L. Ren, K. Yang, L. Guo and H.-w. Chai, *Materials Science and Engineering: C*, 2012, **32**, 1204-1209.

9 F. Martin, T. Linden, D. M. Katschinski, F. Oehme, I. Flamme, C. K. Mukhopadhyay, K. Eckhardt, J. Troger, S. Barth, G. Camenisch and R. H. Wenger, *Blood*, 2005, **105**, 4613-4619.

10 L. Finney, S. Vogt, T. Fukai and D. Glesne, *Clinical and experimental pharmacology & physiology*, 2009, **36**, 88-94.

11 P. Habibovic and J. E. Barralet, *Acta biomaterialia*, 2011, **7**, 3013-3026.

12 J. P. Rodriguez, S. Rios and M. Gonzalez, *Journal of cellular biochemistry*, 2002, **85**, 92-100.

13 A. Ewald, C. Kappel, E. Vorndran, C. Moseke, M. Gelinsky and U. Gbureck, *Journal of biomedical materials research. Part A*, 2012, **100**, 2392-2400.

14 M. C. Cortizo, M. F. De Mele and A. M. Cortizo, *Biological trace element research*, 2004, **100**, 151-168.

15 W. Ran, Z. H. Tian, B. Guo, D. L. Shu, K. H. Nan and Y. J. Wang, *Biomedical materials*, 2009, **4**, 055003.

16 C. M. Han, H. E. Kim, Y. S. Kim and S. K. Han, *Journal of biomedical materials research. Part B, Applied biomaterials*, 2009, **90**, 165-170.

17 H. Ishizawa and M. Ogino, *Journal of biomedical materials research*, 1995, **29**, 65-72.

18 P. Lu, L. Cao, Y. Liu, X. Xu and X. Wu, *Journal of biomedical materials research. Part B, Applied biomaterials*, 2011, **96**, 101-109.

19 J. H. Jo, J. Y. Hong, K. S. Shin, H. E. Kim and Y. H. Koh, *Journal of biomaterials applications*, 2012, **27**, 469-476.

20 J. Li, W. Zhang, Y. Qiao, H. Zhu, X. Jiang, X. Liu and C. Ding, *Journal of Materials Chemistry B*, 2014, **2**, 283-294.

21 X. Jiang, J. Zhao, S. Wang, X. Sun, X. Zhang, J. Chen, D. L. Kaplan and Z. Zhang, *Biomaterials*, 2009, **30**, 4522-4532.

22 J. Li, X. Liu, Y. Qiao, H. Zhu, J. Li, T. Cui and C. Ding, *RSC Advances*, 2013, **3**, 11214-11225.

23 N. WONgPiSuTPaiSaN, N. ViTTayakOrN, A. Ruangphanit and W. Pecharapa, *Sains Malaysiana*, 2013, **42**, 175-181.

24 V. V. Atuchin, V. G. Kesler, N. V. Pervukhina and Z. Zhang, *Journal of Electron Spectroscopy and Related Phenomena*, 2006, **152**, 18-24.

25 Z. Q. Yao, Y. Ivanisenko, T. Diemant, A. Caron, A. Chuvilin, J. Z. Jiang, R. Z. Valiev, M. Qi and H. J. Fecht, *Acta Biomaterialia*, 2010, **6**, 2816-2825.

26 A. Dupraz, T. P. Nguyen, M. Richard, G. Daculsi and N. Passuti, *Biomaterials*, 1999, **20**, 663-673.

27 C. Wagner and G. Muilenberg, *Handbook of X-ray photoelectron spectroscopy*, Perkin-Elmer, 1979.

28 Y. Han, D. Chen, J. Sun, Y. Zhang and K. Xu, *Acta Biomaterialia*, 2008, **4**, 1518-1529.

29 X. Zhu, J. Chen, L. Scheideler, R. Reichl and J. Geis-Gerstorfer, *Biomaterials*, 2004, **25**, 4087-4103.

30 W. Zhang, K. Du, C. Yan and F. Wang, *Applied Surface Science*, 2008, **254**, 5216-5223.

31 G. Moretti, G. Fierro, M. Lo Jacono and P. Porta, *Surface and interface analysis*, 1989, **14**, 325-336.

32 Z. Hussain, M. Salim, M. Khan and E. Khawaja, *Journal of non-crystalline solids*, 1989, **110**, 44-52.

33 G. P. Dubey and S. Ben-Yehuda, *Cell*, 2011, **144**, 590-600.

34 S. B. Goodman, Z. Yao, M. Keeney and F. Yang, *Biomaterials*, 2013, **34**, 3174-3183.

35 K. G. Neoh, X. Hu, D. Zheng and E. T. Kang, *Biomaterials*, 2012, **33**, 2813-2822.

36 L. H. Li, Y. M. Kong, H. W. Kim, Y. W. Kim, H. E. Kim, S. J. Heo and J. Y. Koak, *Biomaterials*, 2004, **25**, 2867-2875.

37 A. Dos Santos, J. R. Araujo, S. M. Landi, A. Kuznetsov, J. M. Granjeiro, L. A. de Sena and C. A. Achete, *Journal of materials science. Materials in medicine*, 2014.

38 C. Gerard, L. J. Bordeleau, J. Barralet and C. J. Doillon, *Biomaterials*, 2010, **31**, 824-831.

39 K. Huo, X. Zhang, H. Wang, L. Zhao, X. Liu and P. K. Chu, *Biomaterials*, 2013, **34**, 3467-3478.

40 X. Liu, P. K. Chu and C. Ding, *Materials Science and Engineering: R: Reports*, 2004, **47**, 49-121.

41 B. Cao, Y. Zheng, T. Xi, C. Zhang, W. Song, K. Burugapalli, H. Yang and Y. Ma, *Biomedical microdevices*, 2012, **14**, 709-720.

42 R. G. Contreras, J. R. Vilchis, H. Sakagami, Y. Nakamura, Y. Nakamura, Y. Hibino, H. Nakajima and J. Shimada, *In vivo*, 2010, **24**, 507-512.

43 L. Yang, S. Perez-Amodio, F. Y. Barrere-de Groot, V. Everts, C. A. van Blitterswijk and P. Habibovic, *Biomaterials*, 2010, **31**, 2976-2989.

44 C. A. Grillo, M. A. Reigosa and M. F. Lorenzo de Mele, *Mutation research*, 2009, **672**, 45-50.

45 W. M. Elshahawy, I. Watanabe and P. Kramer, *Dental materials : official publication of the Academy of Dental Materials*, 2009, **25**, 1551-1555.

46 K. Kelland, *Clin. Infect. Dis.*, 2011, **52**, I-II.

47 J. Li, G. Wang, H. Zhu, M. Zhang, X. Zheng, Z. Di, X. Liu and X. Wang, *Sci. Rep.*, 2014, **4**, 4359.

48 O. Sharifahmadian, H. R. Salimijazi, M. H. Fathi, J. Mostaghimi and L. Pershin, *Surface and Coatings Technology*, 2013, **233**, 74-79.

49 K. Anselme, A. Ponche and M. Bigerelle, *Proceedings of the Institution of Mechanical Engineers. Part H, Journal of engineering in medicine*, 2010, **224**, 1487-1507.

50 K. Anselme, *Biomaterials*, 2000, **21**, 667-681.

51 C. Wu, Y. Zhou, M. Xu, P. Han, L. Chen, J. Chang and Y. Xiao, *Biomaterials*, 2013, **34**, 422-433.

52 A. Weidemann and R. S. Johnson, *Cell death and differentiation*, 2008, **15**, 621-627.

53 R. C. Riddle, R. Khatri, E. Schipani and T. L. Clemens, *Journal of molecular medicine*, 2009, **87**, 583-590.

54 W. Gotz, C. Reichert, L. Canullo, A. Jager and F. Heinemann, *Annals of anatomy - Anatomischer Anzeiger : official organ of the Anatomische Gesellschaft*, 2012, **194**, 171-173.

Table 1. Primers for real-time polymerase chain reaction (PCR).

Gene	Prime sequence (F, forward; R, reverse)	Product size (bp)	Accession number
β-Actin	F: AGGGAGTGATGGTTGGAATG	107	NM_031004.2
	R: GATGATGCCGTGTTCTATCG		
OPN	F: CAAGCGTGGAAACACACAGCC	165	NM_012881.2
	R: GGCTTTGGAACTCGCCTGACTG		
BMP-2	F: ATGGGTTTGTGGTGGAAGTG	167	NM_017178.1
	R: TGTTTGTGGAGTGGATGTC		
COL-1	F: GGCAAGAACGGAGATGATG	143	NM_053304.1
	R: TCCAAACCACTGAAACCTCTG		
HIF-1α	F: CGATGACACGGAAACTGAAG	122	NM_024359.1
	R: CAGAGGCAGGTAATGGAGACA		
VEGF	F: TTGAGTTGGGAGGAGGATGT	115	NM_001110333.1
	R: TGGCAGGCAAACAGACTTC		

Figure captions

Scheme 1. Schematic fabrication procedures of bioactive Cu-incorporated TiO_2 coatings on Ti surface by combining micro-arc oxidation and hydrothermal treatment together.

Figure 1. Surface morphology of the micro-arc oxidized TiO_2 coating (**A-B**) and Cu-incorporated TiO_2 coatings (**C-D** for 10nM-Cu and **E-F** for 100nM-Cu) examined by SEM at low and high magnifications, respectively.

Figure 2. XRD patterns of the micro-arc oxidized TiO_2 coating and Cu-incorporated TiO_2 coatings.

Figure 3. Surface XPS full spectra of TiO_2 coatings with/without Cu doping (**A**) and high-resolution XPS spectra of Ti 2p (**B**), O 1s (**C**), P 2p (**D**), Ca 2p (**E**) and Cu 2p (**F**), accompanied by the release characteristics of P, Ca and Cu ions (**G-I**).

Figure 4. Typical photographs of recultivated E. coli colonies on agar (**A**) and the corresponding antimicrobial ratios (**B**), accompanied by the SEM morphology of E. coli on TiO_2 coating (**C-D**), 10nM-Cu (**E-F**) and 100nM-Cu (**G-H**) with the seeded bacteriaL concentration being 10^7 CFU/mL. The red arrows correspond to the

partially enlarged rectangular regions. All the data are expressed as means ± SD and n = 3.

Figure 5. Results of MTT assay showing the proliferation and viability of BMSCs cultured on the micro-arc oxidized TiO_2 coatings with/without Cu doping.

Figure 6. SEM morphology of BMSCs cultured on the TiO_2 coating (**A**), 10nM-Cu (**B**) and 100nM-Cu (**C**) showing the cell adhesion and spreading abilities.

Figure 7. Immunofluorescence detection of cell morphology. Actin filament (cytoskeleton) stained green, while the cell nuclei stained blue. "Merge" represent merged images of the two fluorochromes for each sample. Scale bar =500 μm.

Figure 8. Alkaline phosphatase (ALP) staining of BMSCs cultured on the TiO_2 coating (**A**), 10nM-Cu (**B**) and 100nM-Cu (**C**), accompanied by the results of quantitative assay (**D**).

Notes: *$p < 0.05$, **$p < 0.01$ versus control TiO_2 group, ##$p < 0.01$ versus 10nM-Cu group.

Figure 9. Gene expression levels of angiogenesis-related markers (**A**, VEGF; **B**, HIF-1α) and osteogenesis-related markers (**C**, OPN; **D**, BMP-2; **E**, Col-1), showing the angiogenic and osteogenic activities of BMSCs cultured on various coatings.

Notes: *$p < 0.05$, **$p < 0.01$ versus control TiO_2 group, ##$p < 0.01$ versus 10nM-Cu group.

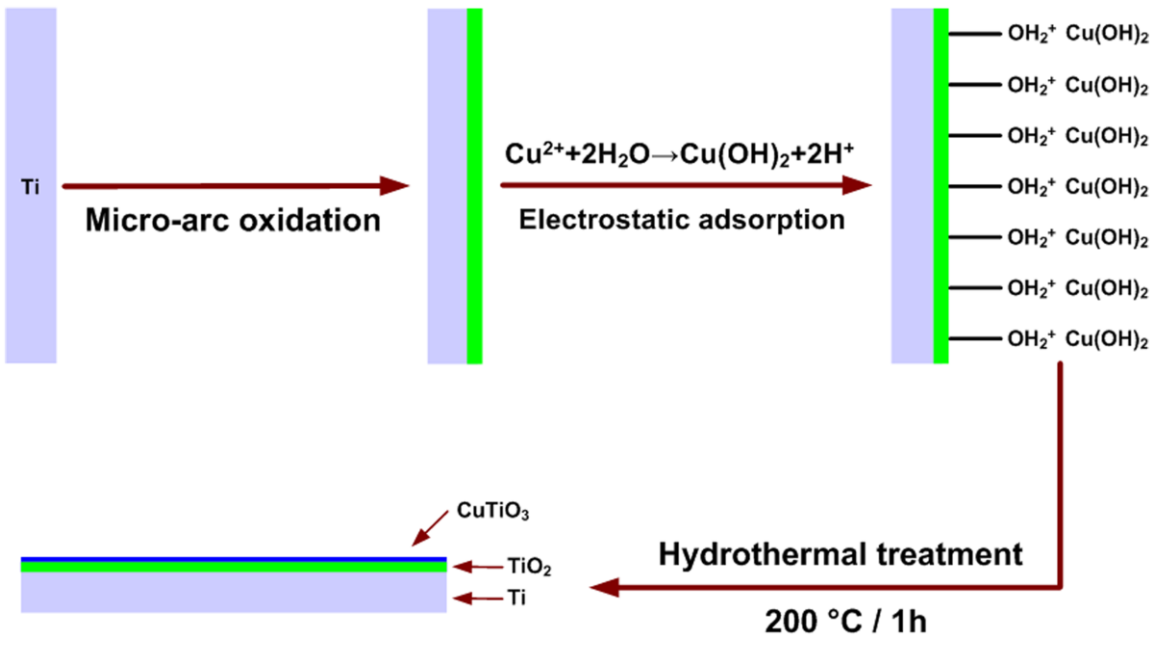

Scheme 1. Schematic fabrication procedures of bioactive Cu-incorporated TiO_2 coatings on Ti surface by combining micro-arc oxidation and hydrothermal treatment together.

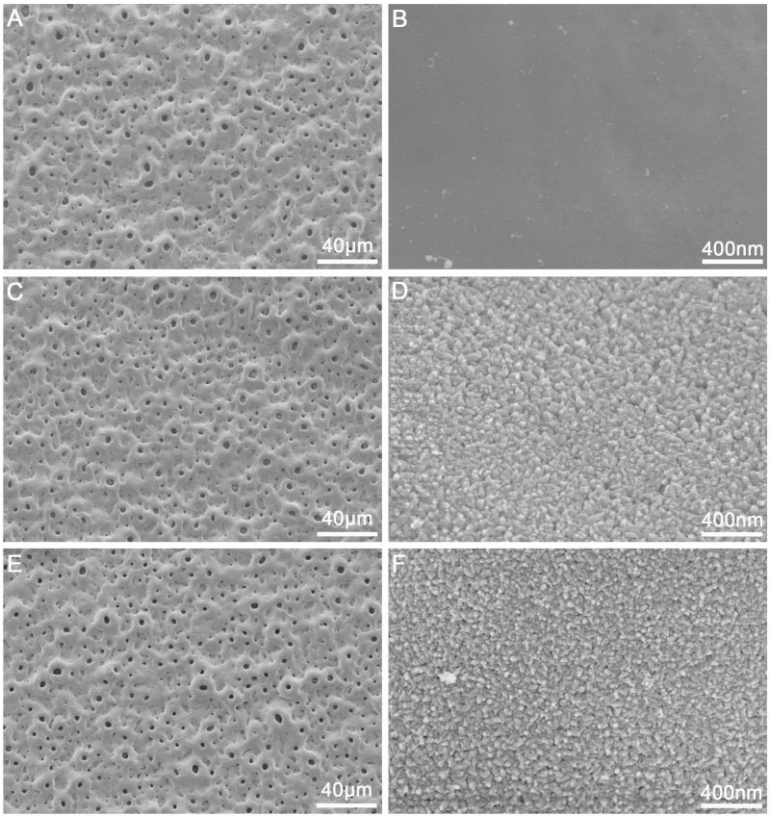

Figure 1. Surface morphology of the micro-arc oxidized TiO_2 coating (**A-B**) and Cu-incorporated TiO_2 coatings (**C-D** for 10nM-Cu and **E-F** for 100nM-Cu) examined by SEM at low and high magnifications, respectively.

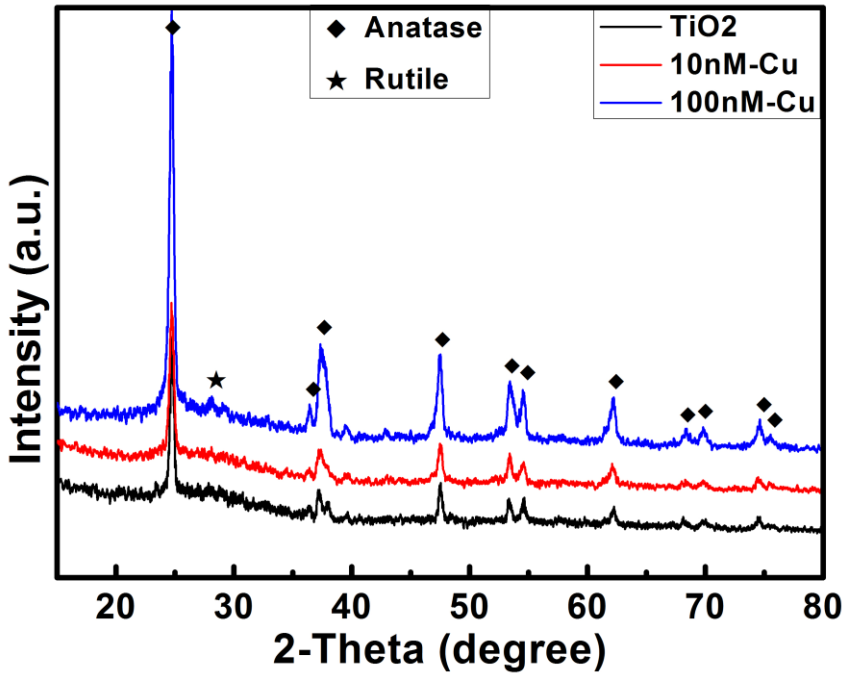

Figure 2. XRD patterns of the micro-arc oxidized TiO_2 coating and Cu-incorporated TiO_2 coatings.

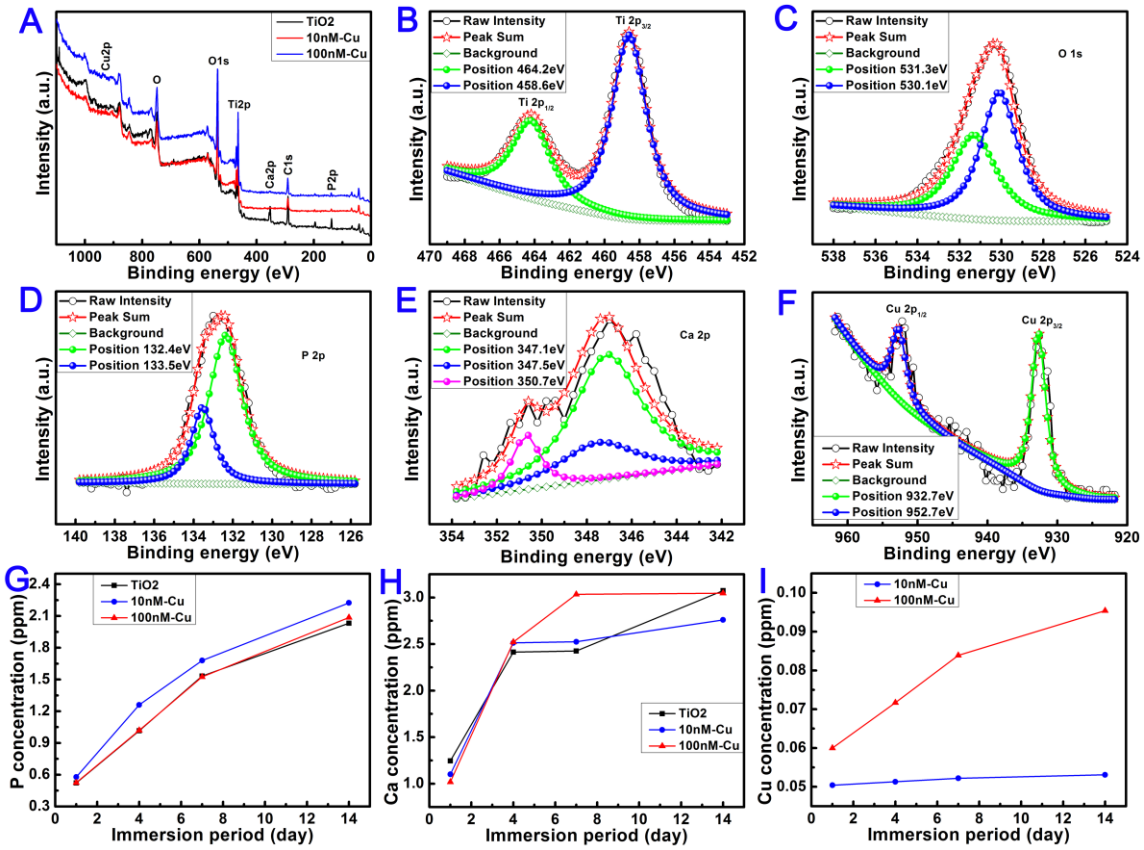

Figure 3. Surface XPS full spectra of TiO_2 coatings with/without Cu doping (**A**) and high-resolution XPS spectra of Ti 2p (**B**), O 1s (**C**), P 2p (**D**), Ca 2p (**E**) and Cu 2p (**F**), accompanied by the release characteristics of P, Ca and Cu ions (**G-I**).

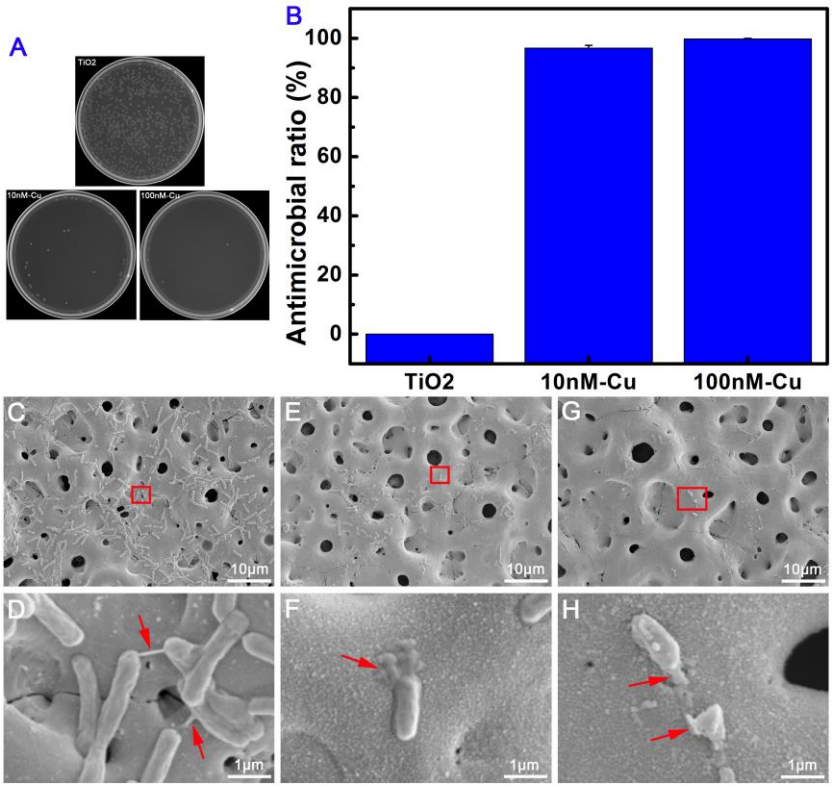

Figure 4. Typical photographs of recultivated E. coli colonies on agar (**A**) and the corresponding antimicrobial ratios (**B**), accompanied by the SEM morphology of E. coli on TiO_2 coating (**C-D**), 10nM-Cu (**E-F**) and 100nM-Cu (**G-H**) with the seeded bacteriaL concentration being 10^7 CFU/mL. The red arrows correspond to the partially enlarged rectangular regions. All the data are expressed as means ± SD and n = 3.

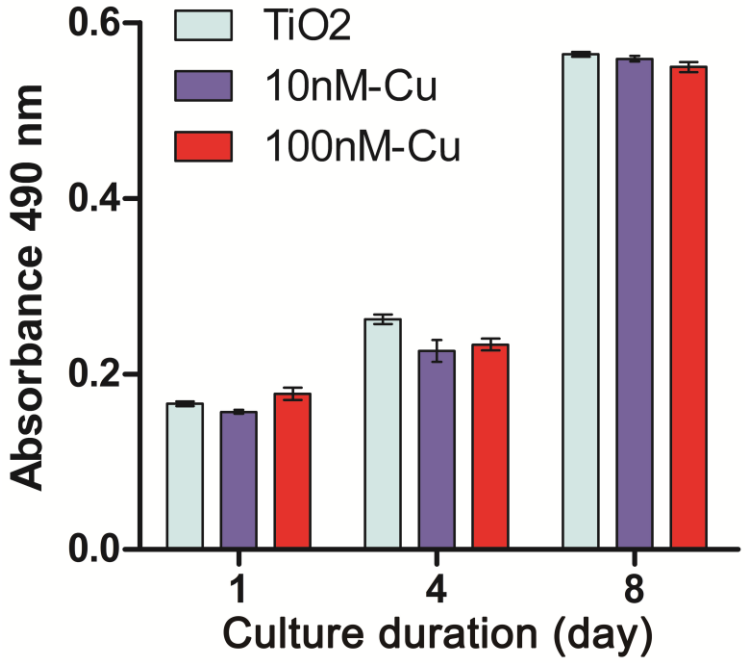

Figure 5. Results of MTT assay showing the proliferation and viability of BMSCs cultured on the micro-arc oxidized TiO_2 coatings with/without Cu doping.

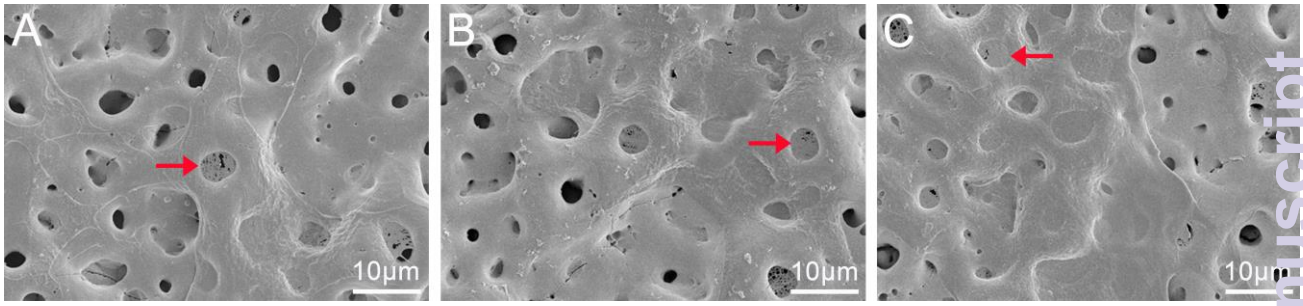

Figure 6. SEM morphology of BMSCs cultured on the TiO_2 coating (**A**), 10nM-Cu (**B**) and 100nM-Cu (**C**) showing the cell adhesion and spreading abilities.

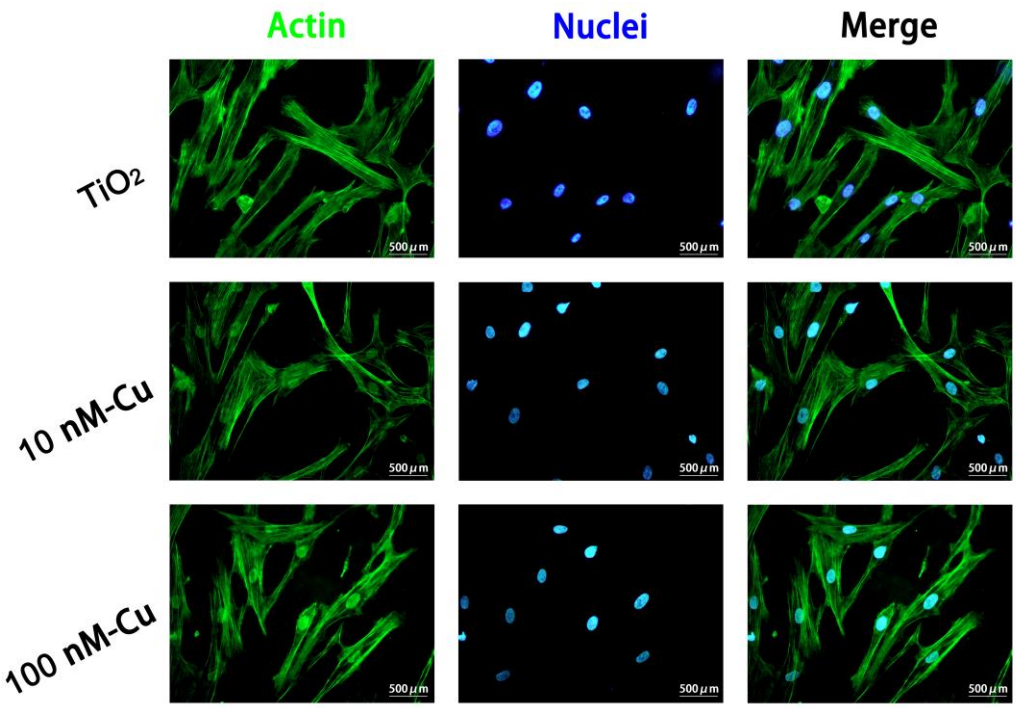

Figure 7. Immunofluorescence detection of cell morphology. Actin filament (cytoskeleton) stained green, while the cell nuclei stained blue. "Merge" represent merged images of the two fluorochromes for each sample. Scale bar =500 μm.

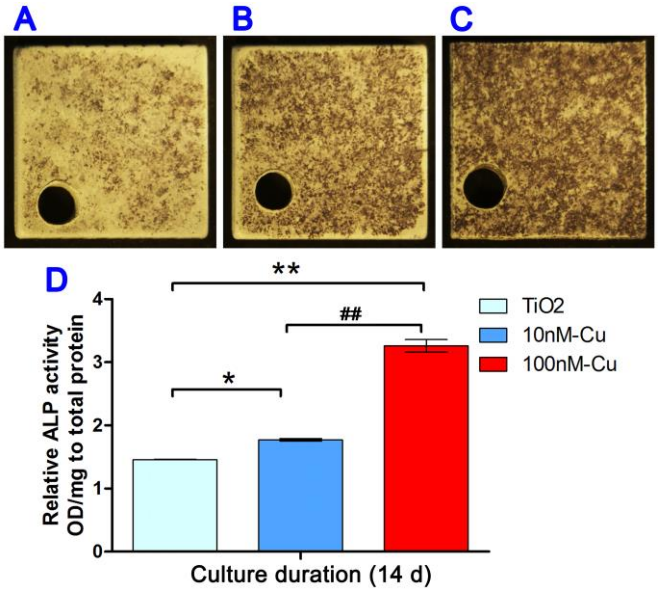

Figure 8. Alkaline phosphatase (ALP) staining of BMSCs cultured on the TiO_2 coating (**A**), 10nM-Cu (**B**) and 100nM-Cu (**C**), accompanied by the results of quantitative assay (**D**).

Notes: *$p < 0.05$, **$p < 0.01$ versus control TiO_2 group, ##$p < 0.01$ versus 10nM-Cu group.

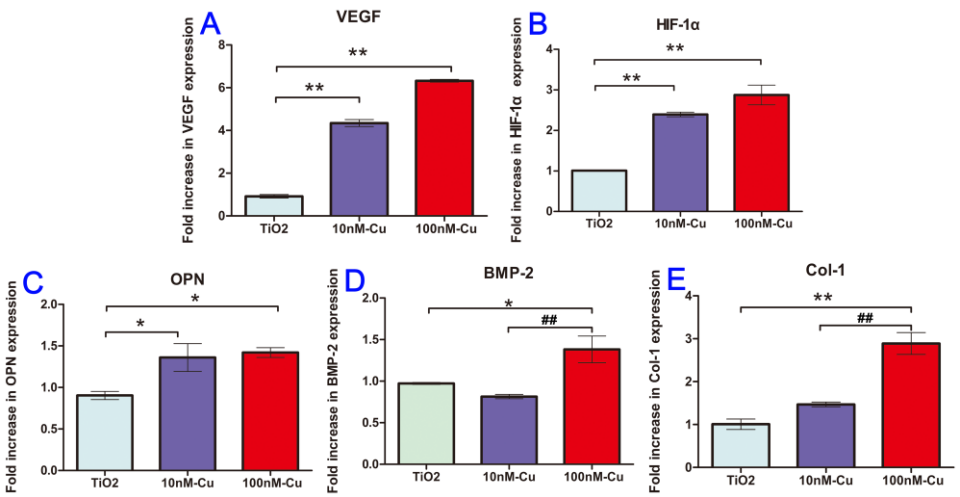

Figure 9. Gene expression levels of angiogenesis-related markers (**A**, VEGF; **B**, HIF-1α) and osteogenesis-related markers (**C**, OPN; **D**, BMP-2; **E**, Col-1), showing the angiogenic and osteogenic activities of BMSCs cultured on various coatings. **Notes:** *$p < 0.05$, **$p < 0.01$ versus control TiO_2 group, ##$p < 0.01$ versus 10nM-Cu group.